WELDABILITY OF COBALT ALLOYS BY HYBRID METHODS

TOMAS HERCIK, MARIAN SIGMUND, PETR HRUBY

FSI VUT Brno, Faculty of Mechanical Engineering, Institute of Welding and Surface Treatment, Brno, Czech Republic.
FCH VUT Brno, Faculty of Chemistry, Institute of Material science, Brno, Czech Republic.

DOI: 10.17973/MMSJ.2021_11_2021009

183936@ vutbr.cz

The article presents the current state of the use of cobalt in various industries and its possible elimination in the field of welding. In this area, it is used in the form of cobalt alloys which are affected by various mechanical and chemical influences. These alloys are produced by the secondary metallurgical area. The primary area is the chemical industry which reserves all the use of cobalt for the production of Li-ion batteries for electric vehicles at an increasing price. The primary area is the chemical industry which reserves all the use of cobalt for the production of Li-ion batteries for electric vehicles at an increasing price. As it becomes unprofitable for other areas, its savings must be sought. From the point of view of welding technology, the solution could be the use of unconventional and hybrid methods that do not require filler material for the connection of elements. Based on these aspects, the methods of a laser beam, electron beam, and combination of a laser beam with TIG method were selected. Verification of the suitability of the use of the mentioned methods was performed on the abrasion-resistant alloy Stellite 6B. The quality of the joints was evaluated by destructive methods such as microstructure, macrostructure, microhardness, and EDS. After evaluating the results of all samples, the hybrid method in the combination of a laser beam and TIG method seems to be the best.

KEYWORDS

Cobalt, cobalt alloys, stellite, unconventional welding, conventional welding.

1 INTRODUCTION

The rare earth element cobalt was detected in 1735 by the Swedish chemist George Brandtn. However, cobalt compounds have been used for centuries due to their blue color. In addition to these applications, a lot of cobalt was found in Egyptian statues and Persian pearl necklaces from 3000 BC. However, before the element itself was discovered, the color was attributed to ores containing copper. These ores were called Kobalt and the real name of the element is taken from them. At the turn of the 20th century, a binary alloy of Co-Cr was investigated by Elwood Haynes, in which he detected high strength and corrosion resistance. Gradually, other strengthening elements such as W and Mo were added. Based on stellar reflection, the alloys were named Stellites from the Latin Stella (star). Further research has confirmed the preservation of mechanical properties even at high temperatures. These attributes have allowed the use in the areas of cutting tools, weld-on layers to increase the wear resistance of surfaces. Developments at the turn of the 1930s and 1940s expanded the use of Stellites for corrosion and high-temperature needs. Co-Cr-Mo alloy has been expanded into the medical and aerospace industries. Today, cobalt compositions are being replaced by nickel or other cheaper compositions. This is due to the global demand for pure elements by the chemical industry which uses it to increase the capacity of lithium-ion batteries. However, the unique properties of alloys (corrosion resistance, abrasion resistance) which they do not lose even at high temperatures, make it impossible to completely replace them. Due to profitability, it will be necessary to look for at least their savings during processing. The most often used uneconomical conventional technologies are TIG and MIG. Cobalt alloys are highly susceptible to hot cracking. The welding process is relatively demanding and requires the use of preheating. In the case of copper's contamination, there is a risk of cracking both in the weld metal (WM) and in the heat affected zone (HAZ). It can prevent these problems and increase the efficiency of the whole process by using unconventional and hybrid technologies (Fig. 1) [DAVIS 2000, SILVA 2019, GUNN 2014, RAMKUMAR 2019, OLSEN 2009].

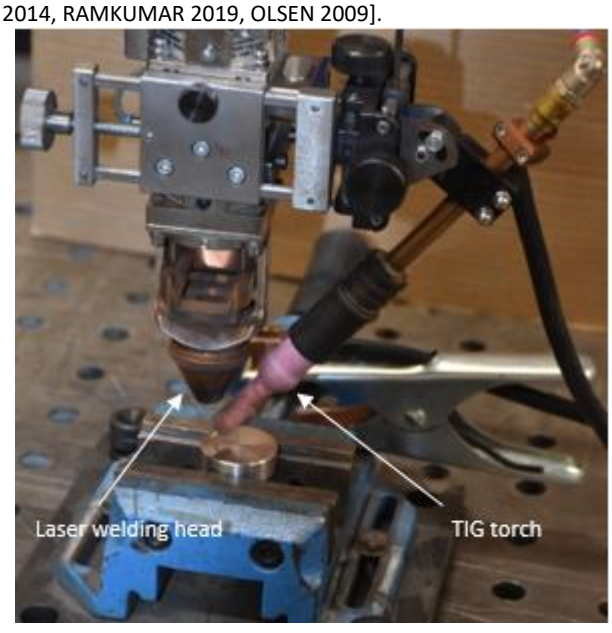

Fig. 1. Hybrid welding technology.

2 CURRENT STATE OF COBALT USE

The properties of cobalt place the element in several countries at a strategic level important for industrial development [GUNN 2014]. Based on the analyzes, a deficit of approximately 885 t was expected in 2018. In the following years, a sharp increase in

the price and reservation of the commodity was expected only for the primary chemical industry which consumes it for the production of lithium-ion batteries for electric cars, telephones, etc. At the beginning of 2020, however, the market showed a declining trend and the value of the commodity was the lowest in the last 2 years (Fig. 2) [RAMKUMAR 2019].

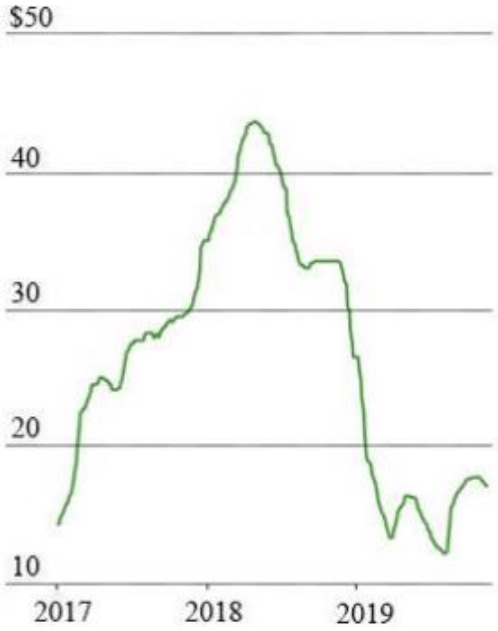

Fig. 2. Graph of cobalt price development [RAMKUMAR 2019].

This steep decline was probably caused by Chinese policy which wanted to use electric cars to solve the local situation with smog. On this basis, it set limits for the sale of petrol engines and subsidies for the purchase of electric cars. However, despite these measures, the amount of demand was not so large. Due to the declining economy, they were forced to abolish limits on the purchase of gasoline engines and reduce subsidies. In 2021, their complete abolition is expected. As the Chinese market represents around 60% of the total global volume of electric cars and the demand for them is not so high, there is a surplus of cobalt in the market. Existing applications, therefore, remain unchanged (Fig. 3). However, this is expected to change in 2024, when cobalt supply should exceed demand. During this period, approximately 47,500 t will be missing and will be pushed out of other applications again [PRATIMA 2019].

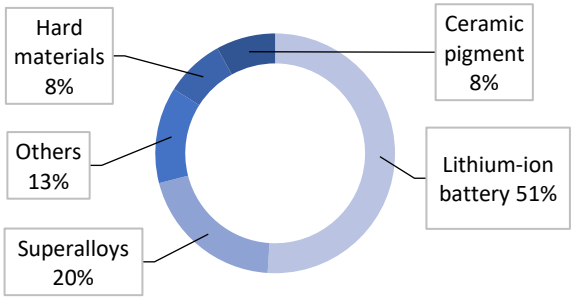

Fig. 3. Graph of the current use of cobalt [GEMC 2019].

3 COBALT ALLOYS

They may also be referred to as superalloys. Their trade and the official name is Stellite. Compared to other alloys, it does not significantly lose its properties such as abrasion resistance, corrosion resistance, and heat resistance with increasing temperature. Their usual application is at a temperature of around 540 ° C. Although each composition can withstand some of these wears to some extent, they are also divided into these 3 groups according to the wear mechanism. Their suitability for a given application is assessed based on chemical composition and method of processing. The chemical composition is mainly the amount of C and the method of processing is the grain size. For applications with mechanical wear, harder compositions are rather recommended which have a higher percentage of carbon and the carbide fraction is therefore larger. Softer compositions have a lower carbon content, a smaller carbide fraction and they are therefore more suitable for refractory applications. The growth and shape of carbides are affected by the rate of cooling and the alloying elements that strengthen the solid solution. To distinguish alloys of given chemical composition, a number is written after the designation Stellite. If the alloy is not in its natural state but is heat-treated, the number is followed by a numerical index. E.g. alloys called Stellite 6B and Stellite 6K are forged compositions extended by amount C. The most common carbides in alloys include M_7C_3 which is rich in Cr, and M_6C, rich in tungsten. The alloys are based on ternary systems Co-Cr-W and Co-Cr-Mo which are derived from the binary system Co-Cr [DAVIS 2019]. To distinguish alloys of given chemical composition, a number is written after the designation Stellite. If the alloy is not in its natural state but is heat-treated, the number is followed by a numerical index. For E.g. alloys called Stellite 6B, and Stellite 6K are forged compositions extended by the amount of C [MATTHEWS 1991].

3.1 Influence of basic alloying elements

The basic characteristic properties of alloys are provided by cobalt with its polymorphic properties (allotropy). It is the ability to change the crystallographic lattice in the solid-state as the temperature changes. Under normal conditions, the grid is hexagonally flat HCP. Between 417 ° C and a melting point of 1493 ° C, the lattice transforms into a surface-centered FCC [GUNN 2014]. In the alloy diagrams, specific phase transformations are denoted as Ɛ-cobalt for HCP and α-cobalt for FCC. As the crystallographic lattice changes, so do the change in magnetic properties. At a temperature of 1121 ° C, the element loses its ferromagnetic properties and acquires paramagnetic properties. Generally, this temperature is referred to as the Curie temperature or point. Compared to iron which has a temperature around 720 ° C, it reaches significantly higher values. Therefore, the crystallographic nature of specific alloys imparts an unstable FCC structure to the alloys with low energy

layered errors. These errors are included among area defects and can be understood as an irregularity in the arrangement of crystallographic planes. The unstable structure together with the low energy of layered defects causes a high yield strength, high curing speed which is important against sliding wear. It also results in a reduction in fatigue damage due to cyclic loading and the ability to absorb stress. These are essential for resistance to cavitation and erosion-corrosion. Another important element is chromium. It is the predominant carbide-forming element in alloys. In addition to carbide formation, it strengthens the strength of the matrix, provides resistance to corrosion and oxidation, reduces the overall density, stabilizes HCP transformation. The ternary system of alloys is enriched with the elements tungsten and molybdenum. Their large atomic size prevents dislocation flow and thus strengthens the strength of the solid matrix. In larger quantities, they can contribute to the formation of carbides and promote their precipitation. Like chromium, they increase corrosion resistance and stabilize HCP transformation. If we consider the applicability of alloys at high temperatures, the melting point of the alloy which is affected by density plays the most important role. It is, therefore, necessary to monitor the mass in high-temperature applications. % of other alloying elements. With elements like rhenium, tantalum density increases, while titanium, aluminum density decrease [DAVIS 2000].

4 EXPERIMENTAL PART

Appropriate welding technologies have been chosen to eliminate filler material. The basic material was abrasion-resistant alloy Stellite 6B. An unconventional method of laser welding was chosen as the first. Based on samples remelted with this technology, suitable welding parameters for other methods were optimized. The samples were further remelted by unconventional electron beam technology and hybrid technology in various laser-TIG configurations. By using an additional heat source of the electric arc of the TIG method, the regulation of heat dissipation was achieved. The suitability of the technology was assessed by destructive tests which include analysis of microstructure and macrostructure, Vickers hardness assessment, and EDS chemical composition analysis.

4.1 Properties of the selected material

The abrasion-resistant Stellite 6B alloy was supplied by the manufacturer KENNAMETAL in the form of a bar metallurgical semi-finished product with a diameter of 34.9 mm. A total of 4 samples with a thickness of 11 mm were cut by machining. The surface of samples were degreased by alcohol. The alloy meets the requirements for use in aerospace, in particular the AMS 5894 specification. Forging is followed by annealing at 1230 ° C and cooling in air. A material sheet with a specific chemical composition was supplied with the alloy, these values are recorded in Table 1 [DAVIS 2000].

C	Cr	Si	W	Fe
0,99	29,47	0,59	3,55	1,25
Co	Ni	Mn	Mo	P/S
Bal.	2,76	1,21	1,35	<0,01/ <0,002

Table 1. Chemical composition in wt. % of Stellite 6B alloy.

The manufacturer guarantees the preservation of mechanical properties even in the case of red heat up to a temperature of 980 ° C. After re-cooling, the mechanical properties are restored. The low coefficient of friction of 0.119 ensures high resistance to seizing. It can even be used in metal-to-metal sliding bearings and in applications where lubrication is not possible. Key features include high resistance to oxidation, corrosive corrosive media, thermal shocks, and cavitation. Due to the combination of corrosion-resistant and abrasion-resistant properties, it is considered an industry standard. It is most often applied by the energy, food, and chemical industries. A specific application of the energy industry is the production of erosion shields for steam turbines which are then able to withstand various wear mechanisms for up to 30 years. The basic general properties are summarized in Table 2. [KENNAMETAL STELLITE]

Density [g·cm-3]	9,39
Melting point [°C]	1265-1354
Thermal conductivity [W·m-1 ·K -1]	14,85
Tensile strength Rm [MPa]	1063
Hardness HRC	36

Table 2. General properties of Stellite 6B alloy.

4.2 Welding by Laser beam

Welding was performed using an optical fiber laser YPG - YSL 2000 with a maximum power of 2 kW with a wavelength of 1070 nm. It is connected by optical cables to the Precitec YRC100 welding head which is located on the robotic arm. On the area of the sample of thickness 11 mm, the remelting was applied on each side at different welding speeds. The used welding conditions are summarized in Table 3.

Welding speed No. 1 [mm·s -1]	20
Welding speed No. 2 [mm·s -1]	10
Laser power [W]	1500
Shield gas [-]	Argon 4.6
Flow of shealding gas [l/min]	18
Focus location [mm]	1

Table 3. Laser welding conditions.

Due to the uniform thermal loading of the base material, the caterpillar was guided through the center of the circular cross-section. The visual appearance of the weld is shown in Fig. 4. The uneven and rough profile of the weld bead is caused by rapid cooling, during which the material was poorly heated. The cause may be a high welding speed or a high gas flow. There is a clear coloration of the temperature-affected area around the weld.

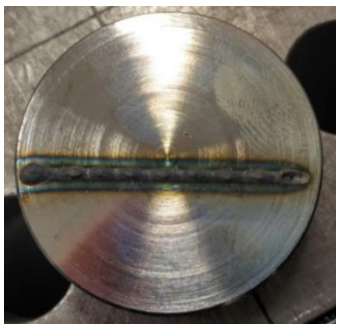

Fig. 4. Weld made by laser beam welding.

4.3 Welding by hybrid technology

Welding was performed by various combinations of a laser beam and TIG arc welding. Either serial or parallel connections can be used for welding. In this case, the aim was regulation of heat dissipation for which are more suitable serial connections (Fig. 5a). The parallel connection (Fig. 5b) is used for joining materials of different thicknesses. The angle α indicates deviation from the laser welding head that regulates the concentration of heat sources. [OLSEN 2009]

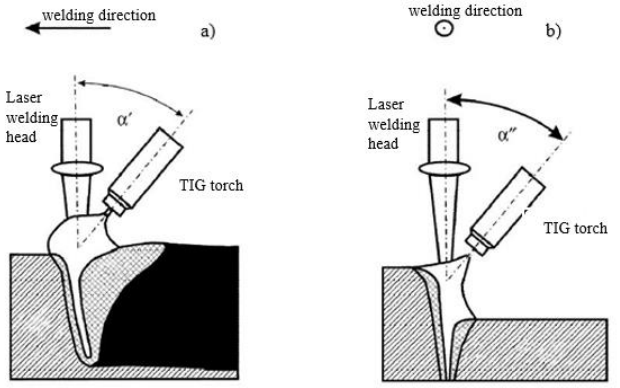

Fig. 5. Scheme of serial (a) and parallel (b) hybrid welding. [OLSEN 2009]

The TIG torch was mounted at an angle and distance to the laser welding head. The same type of laser welding head and the laser itself was used in the previous case. The source of el. a current of the TIG method was the Fronius Magic Wave 1700 Job inventory with a current range of 3-170 A and an operating voltage of 10.1 - 16.8 V. This technology produced a total of two samples with different welding configurations with the designation sample No. 3 and sample No. 4. The laser parameters are derived from the previous method and in both cases are constant. The variables are only the current values of the TIG method. The conditions of hybrid welding are summarized in Table 4.

LASER conditions	
Welding speed [mm·s -1]	10
Laser power [W]	1500
Shield gas [-]	Argon 4.6
Focus location [mm]	1
TIG conditions	
Electrode polarity [-]	DC-
Type of electrode [-]	WT20 (red)
Voltage [V]	12,1
Current for sample No. 3 [A]	60
Current for sample No. 4 [A]	100
Deviation from the laser welding head [°]	45
The distance of the electrode from the laser [mm]	2
The distance of the electrode from the surface [mm]	2

Table 4. Hybrid welding conditions.

Surface of sample No. 3 (Fig. 6b) in the Laser-TIG configuration was remelted first. The welding process took place continuously without delay. The action of both heat sources, therefore, took place simultaneously. This setting aimed to reheat the material to the temperature after welding 250 ° C. For sample No. 4 (Fig. 6a) the TIG-Laser configuration with delay was set. First, the TIG method was passed, followed by laser welding after 5 s. In this case, the goal was to evenly heat the material and reheat it to 300 ° C. A thermal camera was used for measure the temperature without the possibility of recording the course of thermal loading. It could only have recorded the current temperature of the sample. In both cases, the cooling did not occur as rapidly as in the previous case. The visual appearance of the caterpillar is thus better than when welding sample No. 3 (Fig. 6b).

Fig. 6. Welds are made by hybrid technology.

4.4 Electron beam welding

The last samples were welded in a vacuum using a MEBW-60/2 electron welder. The sample surface was remelted on each side. The process parameters were matched the parameters of the laser beam. The process was performed with the same welding parameters as for laser welding (welding speed, laser power). The sample was placed in a vacuum chamber where a weld was performed. After aeration of the chamber, the sample was rotated and a second weld was applied. In each case, the process was accompanied by an unusual crack. This corresponds to the visual appearance of the weld beads (Fig. 7).

Fig. 7. Welds are made by electron beam welding.

4.5 Evaluation of macrostructure

A weld bead was produced to sample on each side at different welding speeds. To highlight the structure, the sample was etched in H_2O_2 + HCl solution.

At first glance, inadmissible defects in the form of cracks and pores are obvious in weld No. 1 (Fig. 8). These defects were caused by the higher welding speed at which heat was dissipated rapidly. It is therefore a type of hot crack that occurred during the solidification of the material due to internal stress. Whereas weld No. 2 (Fig. 9) made at a lower speed shows only micropores. The heat source of the laser beam introduced a larger amount of heat into the weld site than in the previous case, and the heat dissipation was therefore slower. The dimensions of the weld metal (WM), the heat affected zone (HAZ), and the depth of the penetration are thus more extensive. The properties of the structure generally depend on the temperature gradient and solidification rates. These aspects also reflect the tendency and size of dendritic grain growth. The size of the dendritic grains is inversely proportional to the temperature gradient. This rule is confirmed by the coarse-grained structure and the low tendency of the grains of weld No. 2 to grow, where the temperature gradient reached lower values than weld No. 1.

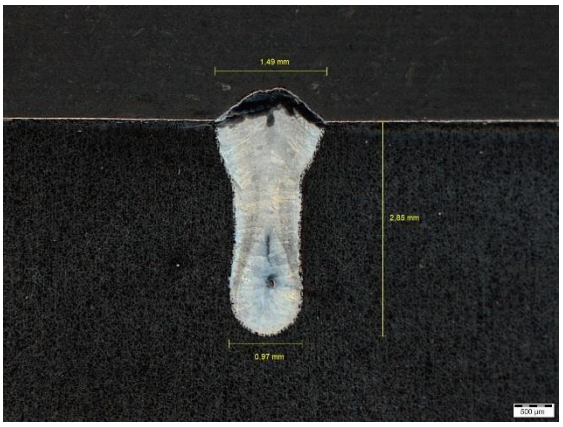

Fig. 8. Macrostructure of sample No. 1.

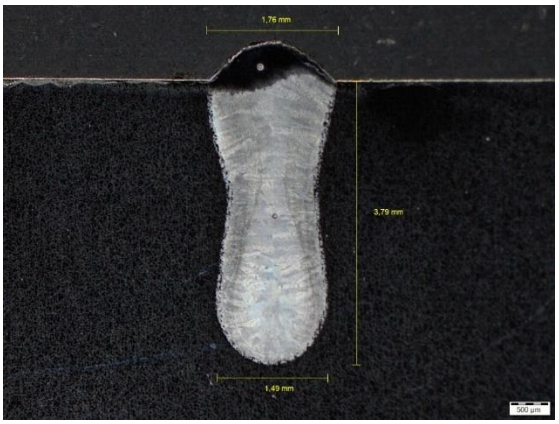

Fig. 9. Macrostructure of sample No. 2.

Color metallography was used to highlight the contrast between the individual phases of the structure of samples 2 and 3 remelted by hybrid technology. The etchant is referred to as Beraha. The concentration of the particular type used was 25 ml H_2O, 25 ml HCl, 0,5 g $K_2S_2O_5$, and 0,7-0,8 g $FeCl_3$. The etching time was 13 s.

From both images of macrostructures, it is clear the oversizing of the welding parameters of the additional heat source and the alignment of the TIG torch. This is indicated by the enlarged right side of the weld metal in the part of the head. The structure of the joints in this area is coarse-grained due to the action of both heat sources. Thus, there is a presumption of worse mechanical properties such as ductility and toughness than in the root part of the joint, where the structure is fine-grained. In sample No. 3 (Fig. 10), where both heat sources acted simultaneously, a macroporous with a size of 460 µm in the root part is visible. The heat affected zone (HAZ) in the left part of the joint is almost negligible. However, in the right part where the TiG burner was concentrated, this area is more extensive. For sample No. 4 (Fig. 11), the heat sources acted with a delay. Thanks to this setting and even thermal load were created and a more homogeneous structure was created than in sample no. 3. The difference in the roughness of the structures in the individual parts of the weld is not so marked. The heat affected zone (HAZ) is almost constant and negligible in each part of the joint.

Fig. 10. Macrostructure of sample No. 3.

Fig. 11. Macrostructure of sample No. 4.

Electron beam samples were prepared under the same conditions as for samples that were remelted by the hybrid method. Weld No. 6 (Fig. 12b) where a lower feed rate was used shows a significant amount of inadmissible defects in the form of hot cracks, which are both longitudinal in the part of the head

and transverse in the weld axis. The changed value of grain growth is again visible on the structures. The main welds are a coarse-grained structure with long and thick grains. The ratio of a temperature gradient to solidification rate was higher for this method. This was probably due to the vacuum in which the whole process took place. Regarding this, there was no such extensive heat dissipation as in previous cases where a protective atmosphere of inert gas was used. Large grains are more prone to cracking as the material solidifies. The beam was focused for a longer time in one place at a lower welding speed, which is reflected in the larger dimensions of the weld than in weld No. 5 (Fig. 12a) where the welding speed was higher. The structure of weld No. 5 contains only a micropore in the root part.

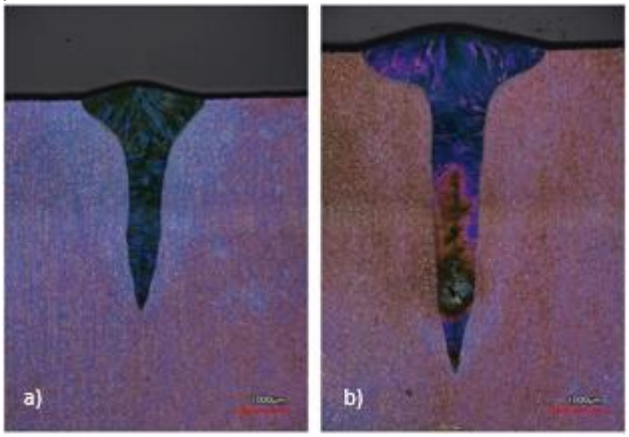

Fig.12. Macrostructure of samples No. 5 (a) and 6 (b).

4.6 Evaluation of microstructure

The microstructure was evaluated only on sample No. 4 remelted in Laser-TIG modification. No filler material was used in any of the samples, so there could be no significant change in structure due to mixing. The mechanism of its creation is thus the same in each case. Fig. 13 shows an image of the microstructure where all areas of the weld are included. The basic material (BM) consists of carbides of the type M_7C_3 (white areas) and $M_{23}C_6$ (black areas at the grain boundaries), which are deposited in a substitution solid solution αCo (FCC grid) [SIGMUND, M 2019**]**. The heat-affected zone (HAZ) is formed by molten or partially melted carbides. This is caused to the different melting points of the individual structural phases. The substitution solid solution αCo has the highest melting point, so it remains almost unchanged in the heat-affected zone. The melting value of individual types of carbides is different. Carbide type M_7C_3 has a melting point in the range 1600-1800 °C, while $M_{23}C_6$ has this value much lower, namely 1000-1100 °C [SHAHROOZI 2018]. This is also confirmed by the image of the microstructure, where there are smaller changes in M_7C_3 carbides at a greater distance from the weld metal. The weld metal (WM) consists of a substitution solid solution ƐCo (HCP lattice) and lamellar eutectic αCo + Cr, which fills the interdendritic space. When etching the sample, the Ɛco substitution solid solution (HCP) had more etching than the αCo substitution solid solution (FCC) [DAVIS 2000]. This structural phase will have lower corrosion resistance. The characteristics of the individual areas were assessed using EDS analysis and binary diagrams Co-Cr and Co-W, so they are only indicative. X-ray phase analysis verification would be necessary for an accurate assertion [MOLLEDA 2006].

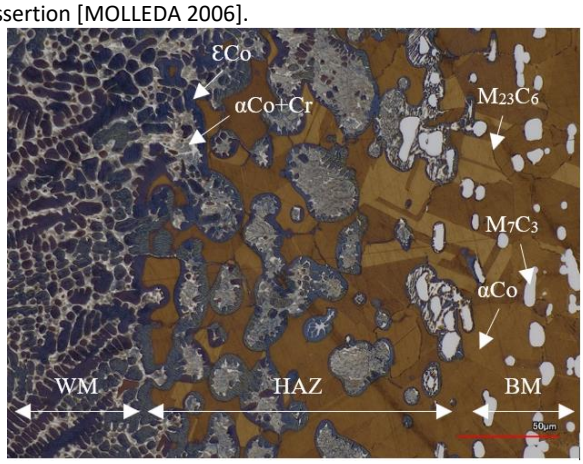

Fig.13. The microstructure of sample No. 4.

4.7 Vicker's hardness evaluation

Hardness measurements were performed only on satisfactory samples without defects. Thus, sample No. 2 and sample No. 3 were included. The measurement was performed in 2 lines that pass through all parts of the joints. Each row contains 21 punctures at a distance of 0.2 mm. The initial requirement was to measure microhardness with a load of HV0.1, but the punctures were too small for evaluation and a load of HV0.5 had to be used. This is therefore a type of hardness test according to Vickerse's at low load. The first line was placed close to the weld head and the second closer to the weld root. It is therefore a type of Vickers hardness test at low load. The first line was placed close to the weld head and the second closer to the weld root.

The measured weld lines of sample No. 2 (Fig. 14) are almost identical. The average values of the lines are 488 (line no. 1) and 498 (line no. 2) HV 0.5. The values need only be taken as an approximation, as there is a considerable amount of carbides in the base material which can distort these values. The graphic display is more accurate. A slight fluctuation in hardness in BM is caused by local fluctuations in carbides. The gradual increase in hardness occurs only during the transition to HAZ were partially melted to molten carbides are saturated. The increase continues until the weld metal where the hardness is again at constant values. The change of hardness is caused by the coarsening of the grain. Because the grain roughness of the weld metal structure in sample No. 1 is constant, the measured lines are identical. Sample No. 4 (Fig. 15) has the same course, but the values of the measured lines differ from the previous sample. The average hardness is 477 (line no. 1) and 464 (line no. 2). The values must be taken only approximately. The hardness of the

lines varies due to the inhomogeneous structure of the weld metal. Both heat sources acted in the part of the head where the heat dissipation was slower and there was room to create a coarse-grained structure with lower mechanical properties. In the root area, however, heat dissipation was faster and a fine-grained structure with better mechanical properties was formed. In the root area, however, heat dissipation was faster and a fine-grained structure with better mechanical properties was formed.

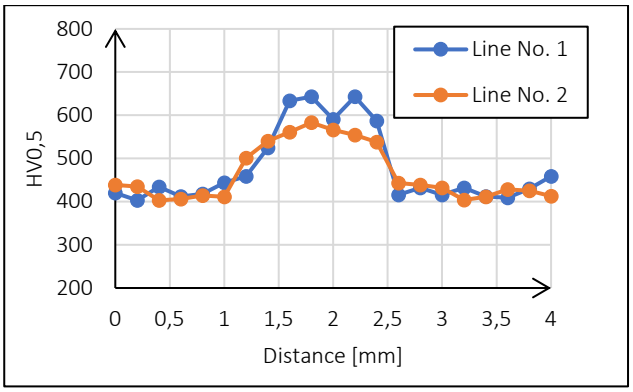

Fig.14. The hardness of sample No. 2.

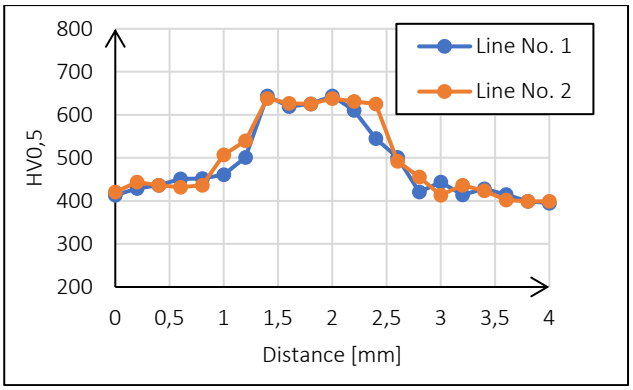

Fig.15. The hardness of sample No. 3.

4.8 Evaluation of chemical composition by EDS analysis

The chemical composition is the same everywhere because no filler material was used. Therefore, only one sample was selected for the investigation, namely sample No. 2 The investigation aimed to verify the chemical composition in all areas of the weld. Based on this, a linear analysis was selected. The type of examined elements was chosen concerning the susceptibility to loss of mechanical and chemical properties in the event of depletion of the element. The greatest emphasis was placed on Cr, which gives the corrosion resistance of the alloy. The decrease can occur either by carbide formation or by evaporation during the melting of the material. However, since the remelted material does not contain any carbides, it can only evaporate in this case. From the measured results (Fig. 16) it is possible to observe a decrease in Co with an increase in Cr in the base material. This is due to the local occurrence of Cr-rich carbides. The gradual transition to the weld metal loses these fluctuations and becomes stable as the carbides dissolve and the structure is homogenized. From the average measured values wt. % indicates that no critical impoverishment occurred in any of the areas.

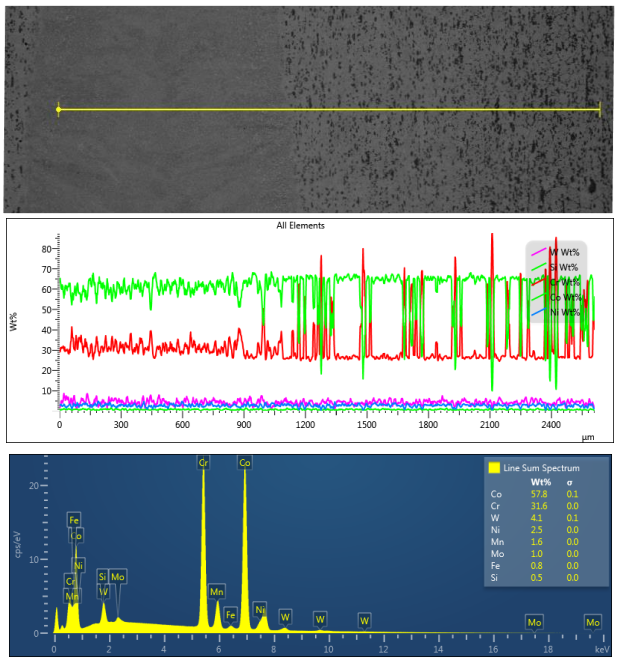

Fig.16. Results of EDS analysis No. 1 of weld No. 2

5 CONCLUSIONS

Cobalt alloys are most often welded by conventional TIG methods using filler material. However, concerning the availability of the element and the range of applications, this technology would be unprofitable in the future. The solution could be to use welding methods that do not need filler material. Based on this requirement, unconventional methods such as electron and laser beam welding were selected. In addition to these methods, hybrid welding in various combinations of laser and TIG arc welding was also chosen. A total of 6 welds were made on 4 samples by various welding parameters using the mentioned methods. The samples were evaluated by destructive methods such as macrostructure, microstructure, Vickers hardness, and EDS chemical analysis. The macrostructure revealed a coarse-grained structure and a large number of unacceptable defects in samples remelted using an electron beam, a laser with higher welding parameters, and hybrid methods in a laser-TIG configuration. They no longer had to be subjected to further testing. As no additive material was used in any of the cases and the structural characteristics were the same everywhere the microstructure could only be examined on one sample. By combining images of the microstructure and EDS analysis, it was found that the weld metal is formed by a substitution solid solution ƐCo (HCP lattice) and a lamellar eutectic αCo + Cr which fills the interdendritic space. Since the phases with Ɛco (HCP lattice) were more etched than the αCo + Cr phases, they will most likely have lower corrosion resistance. The heat-affected zone consists of partially melted to molten

carbides (M7C3, M23C6) which are deposited in a substitution solid solution of αCo (FCC lattice). The Vickers hardness test compared suitable samples welded with lower laser welding parameters and hybrid technology in a TIG laser configuration. Regarding the regulation of heat dissipation using an additional heat source by the TIG method, the sample achieved better mechanical properties and was marked as satisfactory. Lastly, a chemical composition test was performed using EDS line analysis due to the possible evaporation of alloying elements. However, the test did not show a significant decrease in elements. Based on these results, it can be stated that the alloy does not significantly lose corrosion resistance even after welding. It loses only mechanical properties due to dissolved carbides in the weld metal. However, the extent of remelting is minimal and can be neglected. Hybrid welding in a TIG-laser modification thus appears to be the best method.

ACKNOWLEDGMENTS

Acknowledgments to Institute of Scientific Instruments of the Czech Academy of Science, where were realized welding and VUT FSI Brno, Institute of Material Science and Engineering, where were realized all evaluated exams and testing. Financial and material support was also provided by FCH/FSI-J-21-7402 project.

REFERENCES

[DAVIS 2000] DAVIS, Joseph, ed. *Nickel, cobalt, and their alloys*. Materials Park, OH: ASM International, c2000. ISBN 0-87170-685-7.

[GEMC 2019] GEMC. Cobalt Demand. Global Energy Metals Corp [online]. [cit. 2021-05-26]. Available: https://www.globalenergymetals.com/cobalt/cobalt-demand/

[GUNN 2014] GUNN, Gus, et al. *Critical metals handbook*. Chichester: American Geophysical Union, 2014. ISBN 978-0-470-67171-9.

[KENNAMETAL STELLITE] KENNAMETAL STELLITE. Stellite 6B. Kennametal Stellite [online]. [cit. 2021-05- 12]. Available: http://www.stellite.com/en/products/stellite-6b.html

[MATTHEWS 1991] MATTHEWS, S. J., et al. Weldability characteristics of a new corrosion and wear-resistant cobalt alloy. *Weld J Res Suppl*, 1991, 70: 331-338.

[MOLLEDA 2006] MOLLEDA, F., J. MORA, F. J. MOLLEDA, E. MORA, E. CARRILLO a B. G. MELLOR. A study of the solid–liquid interface in cobalt base alloy (Stellite)coatings deposited by fusion welding (TIG). *Materials Characterization* [online]. 2006, 4-5(57), 227-231 [cit. 2021-6-5]. ISSN 1044-5803. Available: https://www.sciencedirect.com/science/article/pii/S1044580306000581

[OLSEN 2009] OLSEN, Flemming Ove. Hybrid Laser-Arc Welding. Woodhead Publishing Limited and CRC, 2009. DOI: 10.1533/9781845696528. ISBN 9781845696528.

[PRATIMA 2019] PRATIMA, Desai. Electric car boom spurs investor scramble for cobalt. Reuters [online]. 2017 [cit. 2018-04-26]. Available: https://www.reuters.com/article/us-cobalt-demand-investors/electric-car-boom-spursinvestor-scramble-for-cobalt-idUSKBN15T1VR.

[RAMKUMAR 2019] RAMKUMAR, Amrith. Battery Metals Slide as Other Commodities Stabilize. In: The Wall Street Journal [online]. New York: Amrith Ramkumar, 2019 [cit. 2021-02-02]. Availble: https://www.wsj.com/articles/battery-metals-sliding-as-other-commodities-stabilize-11574254801?mod=searchresults&page=1&pos=18.

[SHAHROOZI 2018] SHAHROOZI, A., et al. Microstructure and mechanical properties investigation of Stellite 6 and Stellite 6/TiC coating on ASTM A105 steel produced by TIG welding process. *Surface and Coatings Technology*, 2018, 350: 648-658.

[SILVA 2019] SILVA, H. R. a V. A. FERRARESI. Effect of cobalt alloy addition in erosive wear and cavitation of coatings welds. *WEAR* [online]. 2019, 426-427, 302-313 [cit. 2021-6-5]. ISSN 0043-1648. Available: https://www.sciencedirect.com/science/article/pii/S004316481930208X

[SIGMUND, M 2019] SIGMUND, M. Plasma overlay welding of a cobalt alloy. MM (Modern Machinery) Science Journal, October 2019, *2019*, page 2982-2986. ISSN 1803-1269

DOI : 10.17973/MMSJ.2019_10_2018132

CONTACT

Ing. Tomas Hercik

FSI VUT Brno, Faculty of Mechanical Engineering, Institute of Welding and Surface Treatment Technology

Technicka 2896/2, Brno, 616 69, Czech Republic

+420739123310, 183936@vutbr.cz,

https://www.vut.cz/lide/tomas-hercik-183936